

# Experimental Evaluation of MPPT Algorithms: A Comparative Study

Majd Chellal<sup>\*‡</sup>, Thiago Fialho Guimarães<sup>\*\*</sup>, Vicente Leite<sup>\*\*\*</sup>

<sup>\*</sup>Superior School of Applied Sciences, BP 165 RP Bel horizon 13000 Tlemcen, Algeria

<sup>\*\*</sup>Technological Federal University of Paraná, Curitiba-PR, 80230-901, Brazil

<sup>\*\*\*</sup>Research Centre in Digitalization and Intelligent Robotics (CeDRI), Polytechnic Institute of Bragança, Campus de Santa Apolónia - 5300-253 Bragança, Portugal

(majdchellal7@gmail.com, thiagofialho.vg@gmail.com, avtl@ipb.pt)

<sup>‡</sup>Corresponding Author; First Author, Road Aquilino Ribeiro N° 2, 5300-087 Bragança, Portugal,

Tel: +351 934 477 681, majdchellal7@gmail.com

*Received: 16.02.2021 Accepted: 11.03.2021*

**Abstract-** Photovoltaic (PV) energy is among the most used renewable sources. Grid-connected PV systems should yield as much energy as possible. However, external influencers such as irradiance and temperature impose a non-linear characteristic of the PV system, which hinder its operation at the maximum power point. Additionally, other factors, such as shading or internal degradation, can change this characteristic by making local maximums appear, which makes it difficult to extract the maximum available power. There are several techniques for maximum power point tracking (MPPT) and very diverse algorithms for this purpose. There are also some published works with comparative studies. However, in most of these works, the comparison is based on a literature review or on simulation. An experimental evaluation of MPPT techniques, from the simplest to the most complex, remains relevant. Thus, this paper presents an experimental analysis of five MPPT algorithms: two of the simplest and widely used (Perturb & Observe and Incremental Conductance) and three of the most complex (Fuzzy Logic Controller, Kalman Filter and Particle Swarm Optimization). The experimental tests were carried out under real test conditions, using Simulink and the dSPACE 1103 real-time controller board. The results show that the five MPPT algorithms are able to track the MPP with a difference of less than 2% in their efficiency under normal operating conditions. This difference increases under shadow effect. The PSO algorithm was the only one able to find the global MPP under the effect of partial shading.

**Keywords** MPPT algorithms; Perturb and Observe; Incremental Conductance; Fuzzy Logic Control; Kalman filter; Particle Swarm Optimization.

## 1. Introduction

Since the past decade, photovoltaic (PV) energy is among the most preferred source over all the other renewable sources, due to its wide range of qualities such as abundance in nature, low maintenance and high power density [1, 2]. However, the efficiency of PV systems is greatly affected by the efficiency of the inverter, the PV modules and the maximum power point tracking (MPPT) algorithms. PV inverters available on the market have achieved a maximum efficiency of 98% [3]. The increase of PV modules efficiency is under way and has been intensely investigated but it depends on complex

manufacturing processes. Instead, improving the efficiency of the MPPT with various control techniques may be an alternative [4]. The main goal of these algorithms is to achieve the maximum power point (MPP) located along the nonlinear P-V characteristic, which depends on the temperature, solar irradiance and shadow situations [5]. Fig. 1 presents a generic P-V curve under normal test conditions containing a unique MPP, and under partial shading conditions, which contains a local MPP (LMPP) and a global MPP (GMPP)[5, 6].

There are about 10 main MPPT techniques [7, 8], and a few dozen variants [9] published in literature. Some of the most recent works [10-12] deal with the integration of conventional

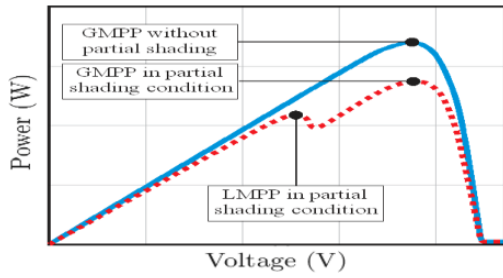


Fig. 1. Generic P-V curves.

and advanced MPPT techniques, since conventional techniques are very complex to implement [13]. In [5], research lacunae and noteworthy remarks are discussed on recently published MPPT algorithms. Most research work focuses on simulation for the purposes of cost and versatility analysis [14, 6], which leads to a lack of information regarding other characteristics. Furthermore, the MPPT based on the Kalman filter has not been sufficiently investigated since only a few simulation studies are known [15–17].

This paper presents an experimental evaluation between different MPPT techniques such as Perturb and Observe (P&O), Incremental Conductance (IC), Fuzzy Logic Controller (FLC), Kalman Filter (KF) and Particle Swarm Optimization (PSO). It compares the performance of these algorithms in terms of oscillation at the MPP, precision of the MPP voltage and shadow effect. The paper brings an experimental perspective, which complement many studies reporting analytical or simulation studies. Furthermore, this paper presents further developments to the previous work [18] with the analysis of the KF algorithm about which there is still lack of information regarding the MPPT capabilities.

The practical implementation of the MPPT algorithms was carried out using a conventional power topology based on a step-up converter followed by a single-phase voltage source inverter under Voltage Oriented Control (VOC) [18]. Both, MPPT and VOC algorithms were implemented in Simulink and tested using the dSPACE 1103 real-time controller board and ControlDesk interface.

2. MPPT Control Algorithms

References [2, 19] present a wide comprehensive review of published algorithms for MPPT, but it does not include the Kalman filter strategy. This section summarizes the MPPT algorithms evaluated in this paper by extending the previous description made in [18] to the Kalman filter technique.

2.1. Perturb and Observe

Perturb and Observe (P&O) technique is the most used and cited in literature due to its simplicity of implementation [19]. The algorithm measures the PV voltage and current to calculate the PV output power. Then, it introduces a perturbation on the voltage reference and observes the effect on the output power. If it increases, the perturbation of the next iteration will continue in the same direction. Otherwise, the direction of the perturbation will be reversed [20-22]. Fig. 2 shows the flowchart of the P&O algorithm.

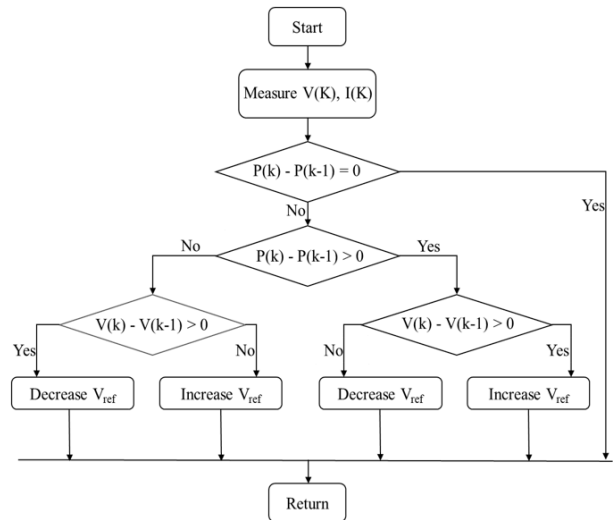


Fig. 2. Flowchart of Perturb and Observe algorithm.

2.2. Incremental Conductance

Considering the convex aspect of the P-V characteristic, the incremental conductance (IC) algorithm is based on the fact that the slope of the P-V curve is equal to zero ( $\frac{\Delta P}{\Delta V} = 0$ ) at the MPP [19]. Eq. (1) presents the operating principle of the IC technique:

$$\begin{cases} \frac{\Delta I}{\Delta V} = -\frac{I}{V} & \text{if } P = MPP \\ \frac{\Delta I}{\Delta V} > -\frac{I}{V} & \text{if } P < MPP \\ \frac{\Delta I}{\Delta V} < -\frac{I}{V} & \text{if } P > MPP \end{cases} \quad (1)$$

The MPP is achieved by comparing the incremental conductance ( $\frac{\Delta P}{\Delta V}$ ) with the instantaneous conductance ( $\frac{I}{V}$ ). Fig. 3 presents the IC technique flowchart, where the algorithm increases or decreases the reference voltage until the condition  $\frac{\Delta I}{\Delta V} = -\frac{I}{V}$  is attained [15].

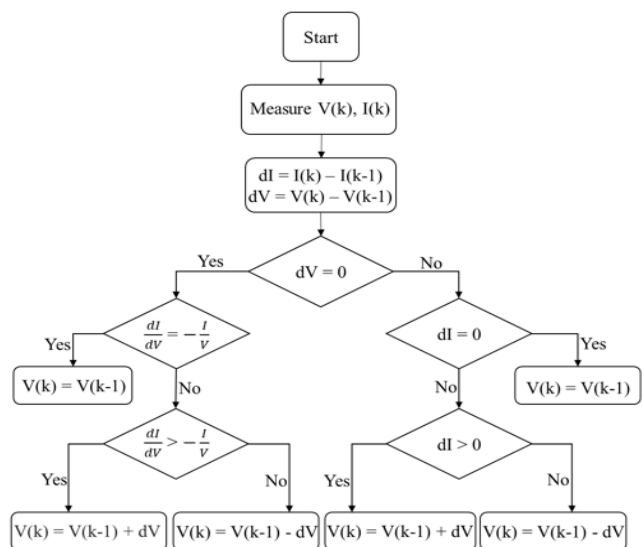


Fig. 3. Flowchart of Incremental Inductance algorithm.

### 2.3. Particle Swarm Optimization

The Particle Swarm Optimization (PSO) algorithm begins with an initial swarm of random particles throughout the research space, where the generation update is completed until the optimal solution is found. Each individual has his own fitness value, which is measured frequently in order to select the optimal individual to continue with the next generation. Each individual has only two values where the first is the personal best ( $P_{best,i}$ ) and the second is the global best ( $G_{best}$ ). The personal best is for each particle while the global best is a unique one for all the particles of the swarm [19, 23]. In short, each particle tries to improve its current location and velocity based on two criteria: the path between its present location and its personal best location, and the distance between its present location and the global best, relative to all the particles. For the MPPT purpose, the operation starts by searching the nearest point to the MPP using the PSO optimization, where the duty cycle of the DC-DC converter represents the position (Particle location) and the output power refers to the fitness function (maximum character function). The PSO flowchart is shown in Fig. 4. The following equations are used to adjust the new position at each iteration, Eq. (3), via the speed equation given by Eq. (2) [24].

$$v_i(k + 1) = w v_i(k) + C_1 R_1 (P_{best,i} - D_i(k)) + C_2 R_2 (G_{best} - D_i(k)) \quad (2)$$

$$D_i(k + 1) = D_i(k) + v_i(k + 1) \quad (3)$$

$D_i$  and  $v_i$  are the duty cycle and the velocity of the particle  $i$ , respectively, and  $C_1$  and  $C_2$  are the acceleration constants.  $w$  refers to the weight of inertia and  $R_1$  and  $R_2$  are random values between 0 and 1.  $P_{best,i}$  is the location with the best fitness of all the visited locations of the particle  $i$ , and  $G_{best}$  is the best position found over all the particles. In this work, the number of initial particles is chosen to be 4,  $C_1$  and  $C_2$  are 1.2 and 2 respectively, and  $w$  equal to 0.4.

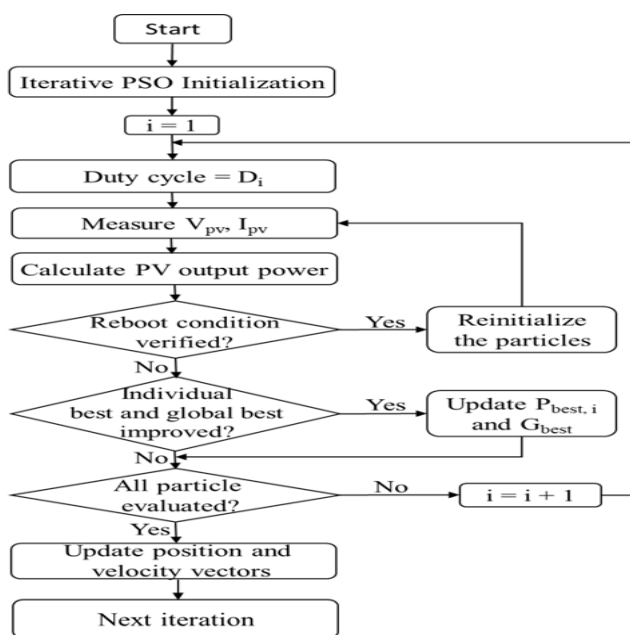


Fig. 4. Flowchart of Particle Swarm Optimization algorithm.

### 2.4. Kalman Filter

The Kalman filter (KF) technique was applied in [16] for MPPT purposes and compared with the P&O algorithm. Recently, other works [15, 17] have done similar studies. Reference [15] presents a comparison between KF and the IC method and in [17] the comparison is with the PSO algorithm. These works present their analysis using simulation results. This work extends the previous experimental research [18] (with P&O, IC and PSO) to the KF and makes the analyses based on experimental results.

The KF is a recursive identification method used for systems described by a state-space representation. However, in this case, it takes into consideration the system ( $r_s$ ) and measurement ( $r_m$ ) noises. The first represents the imperfections of the modeling process and controllers. The second represents the imperfections of measurements. This stochastic state-space representation is described by the following equations [25]:

$$x(k + 1) = Ax(k) + Bu(k) + r_s(k) \quad (4.a)$$

$$y(k) = Cx(k) + r_m(k) \quad (4.b)$$

The first is the state equation and the second is the output equation, where  $u$  and  $y$  represent, respectively, the input and output of the system. The state vector is composed by only one state variable: the PV string output voltage reference. This is the reference for the input voltage of the step-up converter as shown in Fig. 5. In a general case, if the matrices  $A$ ,  $B$  and  $C$  are constant, each state variable of the state vector  $x$  do not depend on other state variables of the same state vector. In that case, the state-space representation (4) is linear and the Kalman filter can be applied. The state-space equations (4) can be applied to the MPPT as demonstrated in [15–17]. Both,  $r_s$  and  $r_m$ , are considered Gaussian and independent sequences. The system output,  $y(k)$ , is the PV string output voltage and the system input,  $u(k)$ , is the slope of the P-V curve,  $\frac{\Delta P}{\Delta V}(k)$ . In this case  $A = B = 1$  and  $B$  is a scaling factor  $M$  as described in [15–17].

The KF is a recursive state estimator method and, in each iteration, it has two steps: prediction and estimation. In the first, it predicts the state variable  $V(k + 1|k)$  and the process covariance value  $P(k + 1|k)$ , considering the information available at instant  $k$  [17]. The Kalman gain  $K(k + 1)$  is then calculated using these predictions. This step requires the process noise covariance value,  $Q$ , and the measurement error value (sensor noise covariance),  $R$ . These values represent the lack of confidence, respectively, in the predicted state and in the measures. Usually these values are obtained by a trial and error process and require some experience.

In the second step, the algorithm estimates the state variable and the process covariance considering the previous information already available at the instant  $k + 1$ , respectively,  $V(k + 1|k + 1)$  and  $P(k + 1|k + 1)$ . The KF algorithm is described in Fig. 6. The two first equations (prediction step) represent the voltage and the process

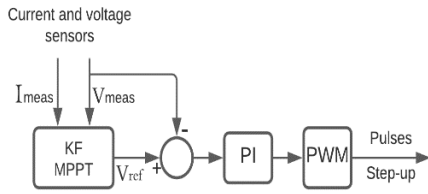


Fig. 5. Step-up converter control using KF for MPPT and a PI controller.

covariance predicted by the algorithm, respectively,  $V_p(k)$  and  $P_p(k)$ . The last three equations represent the estimation step. The computation of the Kalman gain  $K(k)$  requires the measurement error covariance value  $R$  and the predicted process covariance value,  $P_p(k)$ , which in turn requires the process noise covariance value  $Q$ . After that, the state variable (step-up input voltage reference) is updated by the Kalman gain times the error between the measured voltage,  $V(k)$ , given by voltage sensor in Eq. (4b), and the predicted voltage  $V_p(k)$ . Finally, the process covariance value is updated at the same iteration, which tends to become closer and closer to zero [16, 17]. The required parametrization used in this work is summarized in Table 2. In this work, the scale factor is chosen to be 1,  $Q$  is equal to 0.25, and  $R$  equal to 0.31.

2.5. Fuzzy Logic Control

A fuzzy logic controller has three stages, fuzzification, inference mechanism and defuzzification as shown in Fig. 7 [26]. The fuzzification passes the real variables to fuzzy variables. The proposed fuzzy controller has two input variables: the voltage variation ( $\Delta V$ ) and the power variation ( $\Delta P$ ) [26]. In an instant of sampling, these variables are expressed as:

$$\Delta V(k) = V(k) - V(k - 1) \tag{5}$$

$$\Delta P(k) = \Delta V(k) \times \Delta I(k) \tag{6}$$

The input signals  $\Delta V$  and  $\Delta P$  are converted to linguistic variables such as PB (big positive), PM (positive medium), PS (positive small), Z0 (zero), NS (small negative), NM (negative medium), NB (large negative) using the association functions. Fig. 8 shows the association functions used to input and output variables [27].

Fuzzy inference uses Mamdani's method and defuzzification is based on the centroid method to calculate the  $\Delta V_{ref}$  output. Fig. 8 shows the rule base used to find the output and Eq. (7) gives the reference voltage for the PI controller ( $V_{ref}$ ) [18].

$$V_{ref} = V \times \Delta V_{ref} \tag{7}$$

On the other hand, in the defuzzification, the fuzzy logic controller output is converted to a controller variable, which is used by the PI controller as the voltage reference ( $V_{ref}$ ). Fuzzy logic controllers are able to work with inaccurate inputs and, therefore, they do not need a precise linear mathematical model, with a higher implementation cost [27].

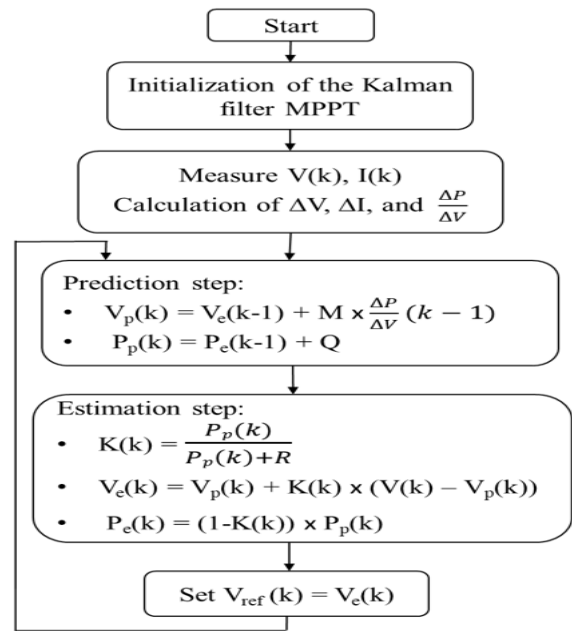


Fig. 6. Flowchart of Kalman Filter algorithm.

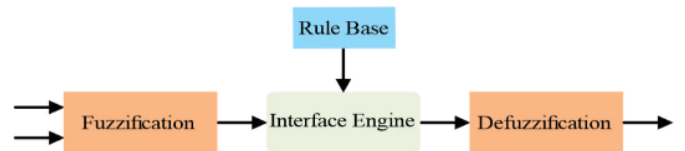


Fig. 7. Flowchart of Fuzzy Logic Controller algorithm.

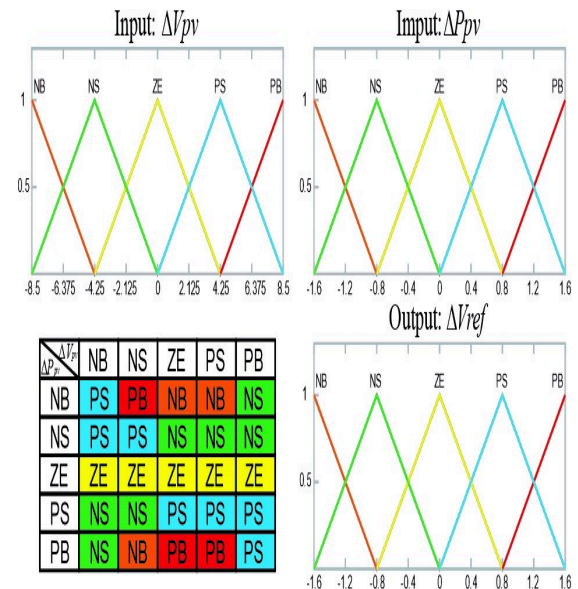


Fig. 8. Membership functions [18].

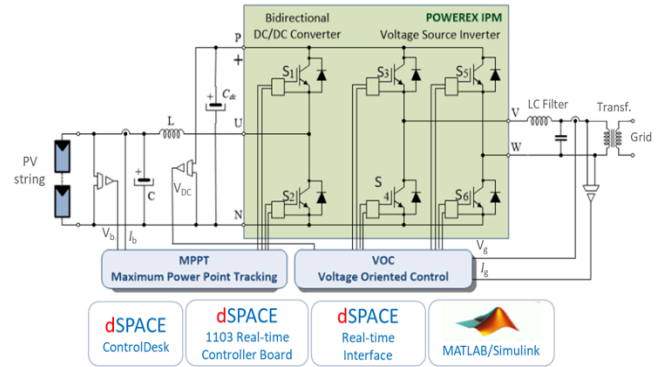
3. Power Topology, Control Strategy and Experimental Set-Up

Fig. 9(a) presents the power topology used in this work. It was implemented using the intelligent power module (IPM) PM75RLA120 from Powerex. This IPM is a three-phase IGBT inverter plus a brake IGBT. The latter is always kept OFF and the three-phase inverter is then configured in order

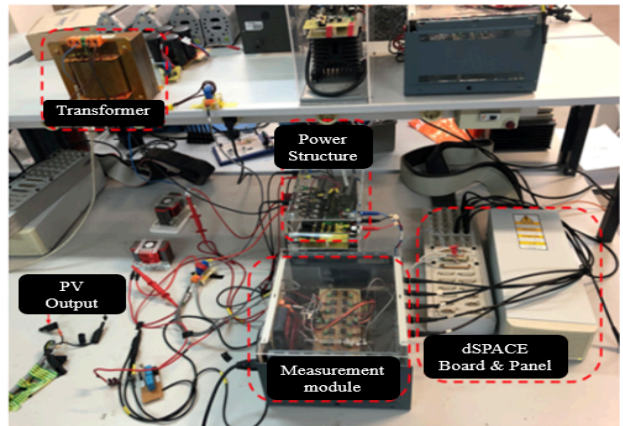
to obtain the desired power topology [28, 29]. Thus, the first leg (U) implements a boost converter by keeping the upper IGBT always OFF. The other two legs (V, W) implement a single-phase voltage source inverter (VSI). Fig. 9(b) shows the experimental set-up. It consists of the power structure, described in the previous paragraph, with an LC output filter and an isolation transformer used for a protection purpose. The measurement module is a signal conditioning interface for data acquisition and signal filtering. The dSPACE 1103 real-time controller board controls the boost converter and the single-phase VSI. The control and user interface are implemented using *Simulink* with *Real-Time Interface* and *ControlDesk*.

The control strategy implements independent control of the boost converter and the VSI. The first controls power extracted from the PV string by setting its operating voltage. The MPPT algorithms described in the previous section generate the reference voltage. Then, the PI controller is responsible for maintaining the output voltage of the PV string equal to the reference voltage given by the MPPT algorithm. Thus, it generates the control voltage for the PWM, as shown in Fig. 5. The second controls the power flow from the PV string to the grid by keeping the DC-link voltage constant at 400 V. For this purpose, the single-phase VSI is controlled using the voltage oriented control (VOC) strategy as in [28, 29]. The implemented VOC of the VSI is shown in Fig. 9(c). The grid current is converted to the fixed orthogonal reference frame  $\alpha\beta$ . For this purpose, a quadrature component is obtained by applying a  $90^\circ$  phase shift. This is carried out by a delay of a quarter of the grid period ( $0.25T$ ) which generates the virtual orthogonal component,  $i_\beta$ . The resulting  $\alpha\beta$  components are orthogonal sinusoidal currents. PI controllers can be used to control sinusoidal currents but there are two well-known drawbacks: they present steady-state errors with sinusoidal reference and are not able to reject disturbances. This is due to the poor performance of the integrative action when the reference is a periodic signal. To overcome this difficulty, the grid current  $\alpha\beta$  components are converted to a  $dq$  reference frame synchronous with the grid voltage. In this new reference frame, the orthogonal components of the grid current are DC quantities and consequently, PI controllers can be used. Therefore, they are able to cancel the steady-state error, at the fundamental frequency of the grid, and improve its dynamic response [28, 29].

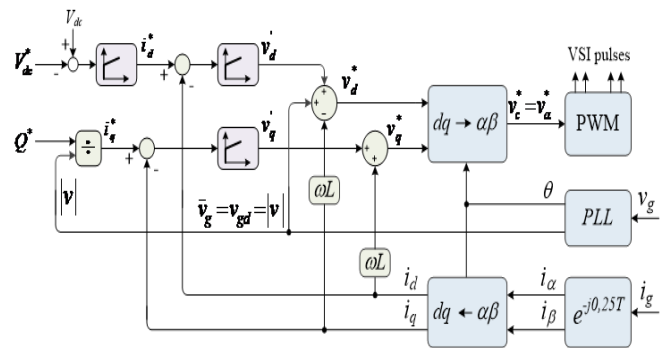
The  $dq$  reference frame rotates with the same angular speed of the grid voltage and current, and the  $d$  axis is permanently aligned with the grid voltage space-phasor. In this way, the grid voltage quadrature component,  $V_{gq}$ , is zero and, therefore, the active and reactive powers are controlled independently by controlling, respectively, the  $d$  and  $q$  current components. The first is controlled by keeping the DC-link voltage constant, as described above, and the second is directly defined, making reactive power compensation possible. In order to obtain the grid voltage angle,  $\theta$ , for reference frame transformation and synchronization, a Phase Locked Loop (PLL) block was implemented as in [28].



(a)



(b)



(c)

Fig. 9. Power structure (a), experimental set-up (b) and VSI control using VOC (c).

Fig. 10 shows the two PV strings used in this work. String A consists of 5 Fluitecnik FTS220P PV modules and string B consists of 3 REC 275PE PV modules. The technical characteristics of the PV modules are shown in Table 1.

Table 1. Characteristics of the PV modules.

String	$P_{max}(W)$	$I_{sc}(A)$	$V_{oc}(V)$	$I_{MPP}(A)$	$V_{MPP}(V)$
A	220	8.30	36.76	7.51	29.38
B	275	9.25	38.70	8.74	31.50



Fig. 10. PV string models [18].

4. Experimental Results

For the experimental tests, the two PV strings described above were used. Under normal operating conditions, all the algorithms were evaluated using PV string A, which has higher power available. The tests were carried on clean days where the irradiation and temperature are almost constant during the time of the test. This PV string is installed on the roof of the laboratory and there is wiring which allows making various configurations (series and parallel) of these modules inside the laboratory. However, for now, it is not very easy nor safe to access the roof. Therefore, due to the difficulty of access for shadow emulation, a second string (B) was placed in front of the laboratory for the tests with shading. Thus, the tests under shading conditions were carried out using PV string B for all algorithms. Immediately before each test, the P-V curve was traced to obtain the MPP.

The PV modules of string B are made up of strings of 20 cells in series with bypass diodes. Thus, to cause a local maximum in the P-V curve, it is enough to shade at least one cell of each string. For this, a semitransparent film was used, as illustrated in Fig. 10.

Each algorithm was tested separately. The MPP voltage, given by each one, was used as a reference voltage for the step-up converter input. The power available on the DC-link was injected into the grid by controlling the single-phase VSI as described in the previous section.

4.1. Tests under normal operating conditions

Fig. 11 shows the experimental results obtained with the MPPT algorithms and string A. At the beginning of the tests, 65 % of the P-V curve is traced in order to identify the MPP. Thus, the control algorithm linearly increases string’s output voltage from 40 V to 150 V, tracing the P-V curve and, therefore, passing through the MPP. Then, the algorithms start with an initial reference voltage of 40 V as shown in Fig. 11(a) to (d). The exception is the PSO algorithm. In this case, the duty cycle increases from 0.4 to 0.9 leading to a linear reduction in the output voltage of the PV string, making it pass through the MPP, as shown in Fig. 11(e).

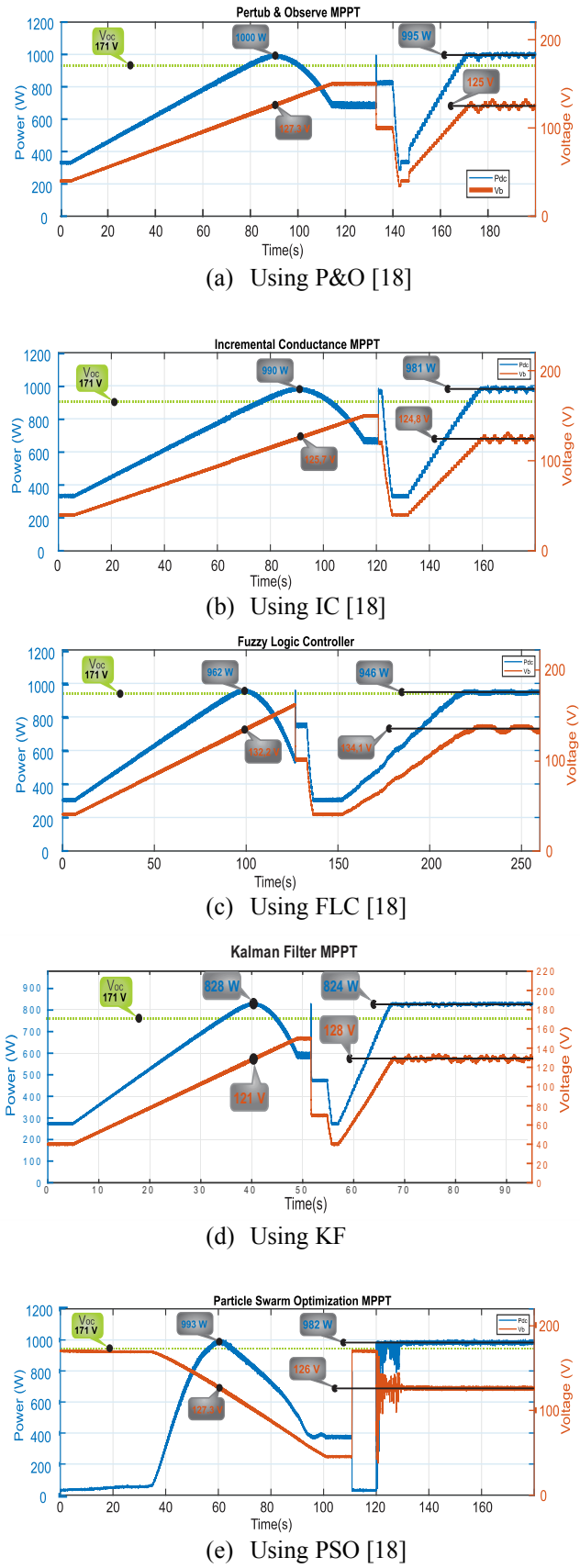


Fig. 11. MPPT algorithms evaluation tests under normal operating conditions.

4.2. Tests under Partial Shading

Fig. 12 shows the experimental results obtained with string B and the shading procedure described previously. The tests were performed as described in the previous section. First, the MPP is identified by tracing the P-V curve and then the algorithms are launched to track the MPP by starting at 40 V.

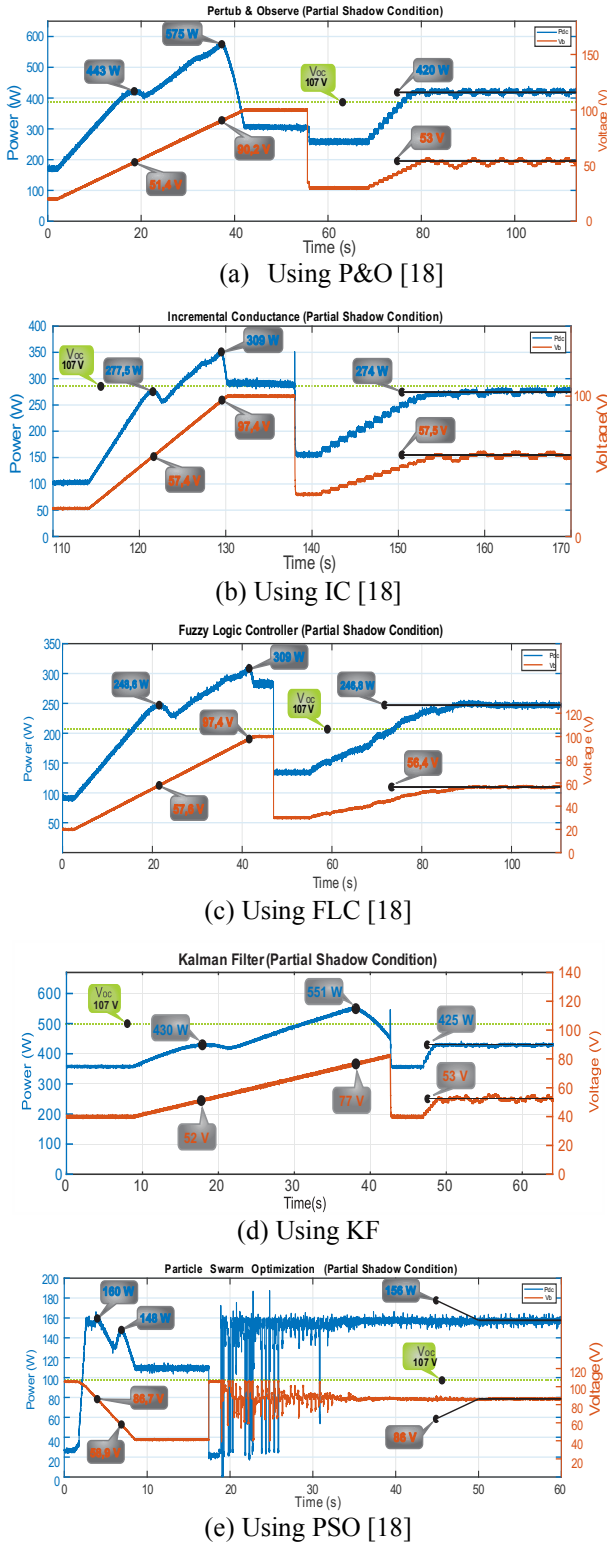


Fig. 12. MPPT algorithms evaluation tests under shading conditions.

5. Discussion

This section discusses the results presented in the previous section. According to the tests carried out, it is possible to compare the performance of each MPPT algorithm in terms of precision in reaching the MPP, oscillation around the MPP, and ability to find the global MPP in shadow situation.

5.1 Oscillation at the MPP

The oscillation around the MPP refers to the difference between the output power maximum and minimum values divided by the power at the MPP previously known, which affects the system efficiency.

Fig. 13 presents a more detailed graphical analysis of the operation of the algorithms after they have already reached the MPP. It shows, graphically, the oscillation in the operating values of power and voltage. The results of this analysis are summarized in Table 2, which presents the power and voltage oscillations of the evaluated MPPT algorithms. The results show that the oscillation is less than 2% with the best results obtained with the PSO and KF algorithms, respectively 0.95% and 1.12%.

It should be noted that MPPT algorithms such as P&O and IC were tested with fixed step increments or decrements in the reference voltage. The size of these steps is a tradeoff between the oscillation magnitude around the MPP and the response time to achieve the MPP. For the purpose of this study, and for the comparison of only conceptual versions, modified implementations as in [12] were not considered.

Table 2. Power and voltage oscillation around the MPP.

Oscilla.	P&O	IC	PSO	FLC	KF
$\Delta P$	1.82%	1.77%	0.95%	1.60%	1.12%
$\Delta V$	4.85%	4.79%	1.61%	3.70%	2.9%

5.2 Ability to achieve the MPP

The efficiency of each algorithm can be evaluated through the difference between the operating voltage imposed by the MPPT algorithm and the MPP voltage previously known (precision). Table 3 presents the ability to achieve the MPP for the evaluated algorithms using Eq. (8), where  $V_{MPP}$  is the MPP voltage given by the P-V curve, and  $V_{MPPT}$  is the voltage where each MPPT technique operates. The  $V_{MPPT}$  value used in Eq. (8) corresponds to the average value of the operating voltage after steady-state has been reached.

$$Precision = 100 \times \left( 1 - \frac{(V_{MPP} - V_{MPPT})}{V_{MPP}} \right) \quad (8)$$

According to the results obtained, efficiency is around 99%, where the best results are obtained with KF and IC algorithms with 99.4% and 99.3% efficiency, respectively.

**Table 3.** Precision of the MPPT techniques.

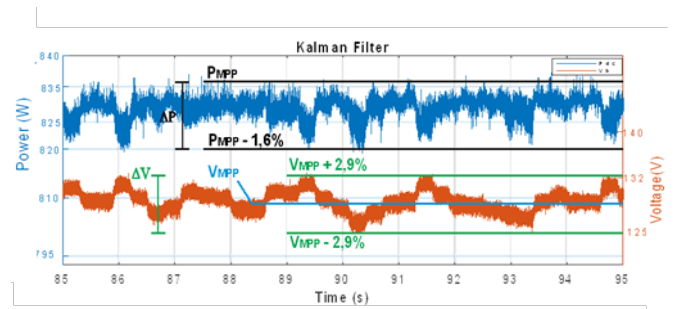
P&O	IC	PSO	FLC	KF
98.2%	99.3%	99.0%	98.6%	99.4%

5.3 Ability to deal with shadow

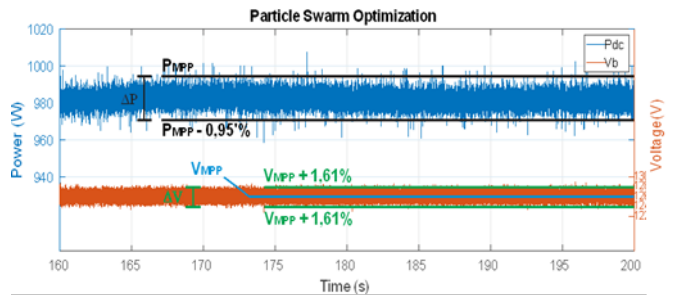
From the analysis of Fig. 12(a) to 12(e), it is clear that only the PSO algorithm is able to reach the global MPP in partial shadow situation, since it is based on the exploratin and exploitation of the research space (starting from 40 V). Following the same protocol, the other MPPT algorithms end operating around a local MPP. Table 4 summarizes these results.

**Table 4.** Ability to deal with partial shadow.

P&O	IC	PSO	FLC	KF
No	No	Yes	No	No



(d) Using KF



(e) Using PSO

**Fig. 13.** Oscillation of the MPPT algorithms at the MPP.

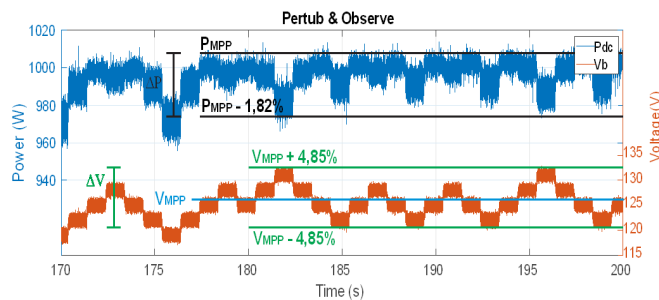
6. Conclusion

This work presented an experimental evaluation of five MPPT algorithms: P&O, IC, PSO, FLC and KF. This comparative study evaluated the performance of the algorithms in relation to 3 parameters: the accuracy of the MPP found in relation to the previously known value; the maximum oscillation of the power extracted from the PV string; and the ability to find the global MPP under the shadow effect. The experimental results show that the KF and IC algorithms operate closer to the MPP than the others. In this case, their efficiency is 99.4% and 99.3%, respectively. However, the PSO algorithm has less oscillation (0.95%) around the MPP compared to the others.

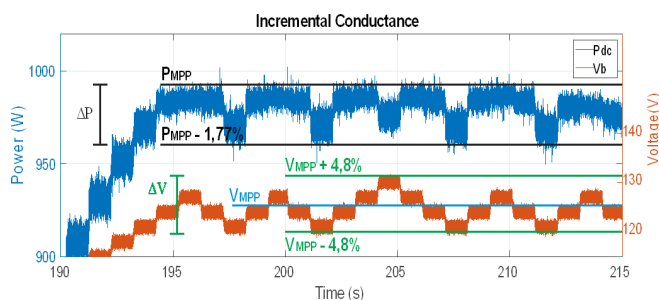
Despite using different methods of different complexity to find the MPP, the difference in efficiency obtained with the techniques was less than 2% under normal operating conditions. However, under partial shadow situations, the efficiency may increase with the PSO since it was the only one that demonstrated to be able to find the global maximum.

References

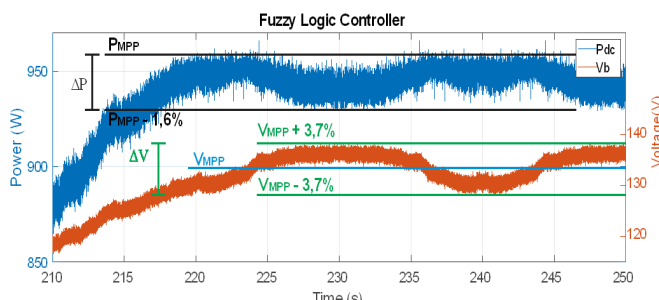
- [1]. P. S. Pai, and S. Beevi, "Dual maximization of solar power for medium power application", 2013 International Conference on Renewable Energy Research and Applications (ICRERA). IEEE, 2013.
- [2]. D. Yousri, T. S. Babu, D. Allam, V. K. Ramachandaramurthy and M. B. Etiba, "A novel chaotic flower pollination algorithm for global maximum power point tracking for photovoltaic system under partial shading conditions", IEEE Access 7 (2019). 121432-121445.
- [3]. S. Wall, H. Xiao-Cong, L. Sha, and J. Xie, "High-efficiency PV inverter with SiC technology", 5th IET



(a) Using P&O



(b) Using IC



(c) Using FLC

- Renewable Power Generation Conference, vol. 12, pp. 149-156, 2017.
- [4]. N. Eswar, "Performance Study of Incremental Conductance and Modified Incremental Conductance MPPT Algorithms for Photovoltaic Applications", *International Journal of Science- Engineering and Technology Research (IJSETR)*, Vol. 5, March 2016.
- [5]. D. Yousri, T. S. Babu, D. Allam, V. K. Ramachandaramurthy, E. Beshr, and M. B. Eteiba. "Fractional chaos maps with flower pollination algorithm for partial shading mitigation of photovoltaic systems", *Energies* 12.18 (2019): 3548.
- [6]. M. Abdulkadir, A. L. Bukar and B. Modu, "Mppt-based control algorithm for PV system using iteration-PSO under irregular shadow conditions", *Arid Zone Journal of Engineering- Technology and Environment*, Vol. 13, February 2017.
- [7]. V. K. Viswambaran, A. Ghani, and E. Zhou, "Modelling and Simulation of Maximum Power point Tracking Algorithms & Review of MPPT Techniques for PV Applications", 5th International Conference on Electronic Devices, Systems and Applications (ICEDSA), pp. 1-4, 6-8 Dec 2016.
- [8]. T. Eswar, and P. L. Chapman, "Comparison of Photovoltaic Array Maximum Power Point Tracking Techniques", *IEEE transactions on energy conversion*, vol. 22, June 2007.
- [9]. H. J. El-Khozondar, and R. J. El-Khozondar, "A review study of photovoltaic array maximum power tracking algorithms", *Renewables: Wind. Water. and Solar*, vol. 3, pp. 1-8, 18 February 2016.
- [10]. A. K. Podder, "MPPT methods for solar PV systems: a critical review based on tracking nature", *IET Renewable Power Generation*, vol. 13, pp. 1615-1632, April 2019.
- [11]. N. Eswar, "Performance Study of Incremental Conductance and Modified Incremental Conductance MPPT Algorithms for Photovoltaic Applications", *International Journal of Science- Engineering and Technology Research (IJSETR)*, Vol. 5, March 2016.
- [12]. A. Belkaid, I. Colak, and K. Korhan. "Implementation of a modified P&O-MPPT algorithm adapted for varying solar radiation conditions", *Electrical Engineering*, 99(3), 2017, 839-846.
- [13]. A. I. Nusaif, and A. L. Mahmood, "MPPT Algorithms (PSO, FA, and MFA) for PV System Under Partial Shading Condition, Case Study: BTS in Algazalia, Baghdad", *International Journal of Smart Grid-ijSmartGrid*, 4(3), 2020, 100-110.
- [14]. J. Cubas, and S. Pindado, "Accurate Simulation of MPPT Methods Performance When Applied to Commercial Photovoltaic Panels", *The Scientific World Journal*, June 2015.
- [15]. S. Motahhir, A. Aoune, A. E. Ghzizal, S. Sebti, and A. Derouich, "Comparison between Kalman filter and incremental conductance algorithm for optimizing photovoltaic energy", *Renewables: Wind. Water. and Solar*, pp. 1-10, vol. 4, 2017.
- [16]. B. O. Kang, "Kalman Filter MPPT Method for a Solar Inverter", *IEEE Power and Energy Conference*. Illinois, pp. 1-5, 2011.
- [17]. O. B. Belghith, L. Sbita, and F. Bettaber, "Maximum Power Point Tracking by the technique of the extended Kalman filter", *International Conference on Green Energy Conversion Systems (GECS)*, pp. 1-5, 2017.
- [18]. T. F. Guimarães and V. Leite, "Analyses of MPPT Algorithms in Real Test Conditions", 9th International Conference on Renewable Energy Research and Application (ICRERA). Glasgow, pp. 164-169, September 2020.
- [19]. P. Bhatnagar, and R. K. Nema, "Maximum power point tracking control techniques: State-of-the-art in photovoltaic applications", *Renewable and Sustainable Energy Reviews* 23, pp. 224-241, July 2013.
- [20]. A. K. Gupta and R. Saxena, "Review on widely-used MPPT techniques for PV applications", 2016 International Conference on Innovation and Challenges in Cyber Security (ICICCS-INBUSH). Noida, pp. 270-273, 2016.
- [21]. A. Belkaid, U. Colak, and K. Kayisli. "A comprehensive study of different photovoltaic peak power tracking methods", 2017 IEEE 6th International Conference on Renewable Energy Research and Applications (ICRERA). IEEE, 2017.
- [22]. M. A. Abdourraziq, M. Ouassaid, M. Maaroufi and S. Abdourraziq, "Modified P&O MPPT technique for photovoltaic systems", 2013 International Conference on Renewable Energy Research and Applications (ICRERA).
- [23]. A. Farayola, Y. Sun, and A. Ali, "ANN-PSO Optimization of PV Systems Under Different Weather Conditions", 2018 7th International Conference on Renewable Energy Research and Applications (ICRERA).
- [24]. K. Ishaque, Z. Salam, M. Amjad and S. Mekhilef, "An improved Particle Swarm Optimization (PSO)-Based MPPT for PV with reduced steady-state oscillation", *IEEE Transactions on Power Electronics*, vol. 27, pp. 3627-3638, August 2012.
- [25]. C. K. Chui, and G. Chen, "Kalman Filtering with Real-Time Applications", Springer International Publishing. Berlin. Germany, 2017.
- [26]. B. Bendib, F. Krim, H. Belmili, M. F. Almi and S. Bolouma, "An intelligent MPPT approach based on neural-network voltage estimator and fuzzy controller, applied to a stand-alone PV system", *IEEE 23rd International Symposium on Industrial Electronics (ISIE)*. Istanbul, 2014, pp. 404-409, 2014.
- [27]. D. Haji and N. Genc, "Fuzzy and P&O Based MPPT Controllers under Different Conditions", 7th International Conference on Renewable Energy Research and Applications (ICRERA). Paris, pp. 649-655, 2018.
- [28]. V. Leite, Â. Ferreira and J. Batista, "Bidirectional vehicle-to-grid interface under a microgrid project", *IEEE 15th Workshop on Control and Modeling for Power Electronics (COMPEL)*. Santander, pp. 1-7, 2014.
- [29]. M. Breve, and V. Leite, "Control of a Bidirectional Single-Phase Grid Interface for Electric Vehicles", *Ibero-American Congress of Smart Cities*. Springer, Cham, 2019.